Variational Quantum Eigensolver for Frustrated Quantum Systems

Alexey Uvarov,[1,*] Jacob D. Biamonte,[1] and Dmitry Yudin[1]

[1] *Skolkovo Institute of Science and Technology, Moscow 121205, Russia*

(Dated: May 5, 2020)

Hybrid quantum-classical algorithms have been proposed as a potentially viable application of quantum computers. A particular example—the variational quantum eigensolver, or VQE—is designed to determine a global minimum in an energy landscape specified by a quantum Hamiltonian, which makes it appealing for the needs of quantum chemistry. Experimental realizations have been reported in recent years and theoretical estimates of its efficiency are a subject of intense effort. Here we consider the performance of the VQE technique for a Hubbard-like model describing a one-dimensional chain of fermions with competing nearest- and next-nearest-neighbor interactions. We find that VQE is able to recover the correlation function of the ground state and the excitation velocities even when the energy convergence is not exact. We also study the barren plateau phenomenon for the Hamiltonians in question and find that the severity of this effect depends on the encoding of fermions to qubits. Our results are consistent with the current knowledge about the barren plateaus in quantum optimization.

Introduction. Based on effective dimensionality reduction of unsorted datasets and the ability to efficiently recognize patterns, neural network algorithms allow one to directly address properties of physical systems with no prior knowledge of the structure of their states. Indeed, with recent advances in machine learning simulation, relatively large spin Hamiltonians of up to a few hundreds entities might be approached [1]. Nevertheless, studying the properties of highly frustrated systems remains a highly non-trivial computational task [2]. At the same time, quantum algorithms have several similarities with various traditional machine learning models. While recent times have seen rapid development in the use of quantum circuits as variational models of quantum machine learning [3], these techniques are still being developed to apply to the simulation of physical systems.

Using variational quantum algorithms is widely considered as a promising approach towards practical application of quantum computers [4–22]. The idea of such algorithms is to delegate as many calculations as possible to a classical device, thereby minimizing quantum resources. A particular example, the variational quantum eigensolver (VQE), represents an implementation of variational quantum circuits which uses a quantum computer to prepare a family of states characterized by a polynomial number of parameters and minimizes the expectation value of a given Hamiltonian within this family. This approach is among the first realized on small- and mid-sized quantum computers [8, 23–25]. Thus, in VQE one aims at finding the ground state of a quantum Hamiltonian with the use of a certain tunable ansatz state that is easy to prepare on a quantum device, but hard to store in classical memory. Using the VQE one can evaluate at least the upper bound of lowest eigenvalue of a given Hamiltonian.

Potential applications of the VQE include quantum chemistry [8, 16, 26–29], condensed matter physics [30–33], and lattice quantum field theory [34], although discrete optimization is also within the scope of variational quantum algorithms [35, 36]. In general, optimization of a local quantum Hamiltonian is a complete problem for complexity class QMA, meaning that particular problems are out of reach even for a quantum computer. However, it is hoped that practical problems can be solved to acceptable tolerance.

In condensed matter physics, frustrated systems with inhomogeneous interactions are hard to analyze owing to extra degrees of freedom to show up. On the one hand, strong electron-electron interactions precludes perturbative expansion over single-electron wave functions. On the other hand, more advanced numerical approaches to strongly correlated systems, *e.g.,* based on dynamical mean-field theory, treat the systems on a purely local manner. Whether modern quantum algorithms can give an edge in analyzing these models is an intensely studied question [30, 37, 38]. In this work, we analyze the performance of VQE for a one-dimensional model of spinless electrons with nearest- and next-nearest-neighbor interactions. This model represents a simple theoretical testbed to explore the physical properties of frustrated systems. Resulting from the competition between two types of interactions, a metallic state emerges even for strongly interacting systems. Interestingly, results of numerical simulations for finite size clusters unambiguously reveal that the ground state does not belong to the Luttinger liquid universality class [39–43].

Moreover, we also address a bottleneck of hybrid algorithms in the regard of the considered model, *i.e.*, we inspect the onset of the so-called plateau regime. One of the more recently identified hurdles when implementing VQE is the so-called *barren plateau* effect [44]. The idea is that the variation of the gradient of any useful cost function decays exponentially with the number of qubits, provided that the quantum circuit used as ansatz in the VQE is long enough to implement an approximate solution. For shorter quantum circuits, the onset of the

plateau regime seems to depend on the geometric locality of the cost function [45]. In VQE, the choice of cost function is motivated by physical problems in question, hence it typically has some kind of locality in its terms. Interestingly enough, the results for the latter are rather sensitive to fermion-to-qubit mapping as we discuss below.

Numerical methodology. Assume that a quantum state $|\psi\rangle = |\psi(\boldsymbol{\theta})\rangle$ can be prepared on a quantum computer, with adjustable real parameters $\boldsymbol{\theta} = (\theta_1, ..., \theta_p)$. Then, by measuring each qubit in a local basis, one can measure expectation values of the type $\langle\psi| \sigma_1 \otimes ... \otimes \sigma_n |\psi\rangle$, where σ_i are drawn from the set of Pauli matrices $\{I, X, Y, Z\}$. We will refer to such observables as Pauli strings. Any Hamiltonian acting on n qubits can be decomposed into a sum of such Pauli strings, and hence we can evaluate the energy $\mathcal{E}(\boldsymbol{\theta}) = \langle\psi| H |\psi\rangle$ with respect to the state prepared on a quantum computer, as long as the number of Pauli strings is polynomial in n. The idea of the VQE is then to find the lowest energy state $|\psi\rangle$ among some set of states that can be prepared on the device. Most often, $|\psi\rangle$ is a state prepared by some quantum circuit with parametrized gates. In this case, the parameters are optimized in a classical computer using the quantum computer as a black box. Noteworthy that under some assumptions on the shape of the ansatz, one may also be able to access derivatives of the cost function [46–49].

For the numerical implementation in this study, we use adaptive moment estimation algorithm (Adam) for gradient descent [50]. In contrast to well known optimization techniques, where an update for all parameters is performed at once with the same learning rate η,

$$\theta_k^{t+1} = \theta_k^t - \eta g_t, \quad g_t = \nabla\mathcal{E}(\theta_k^t), \tag{1}$$

a distinctive feature of the Adam approach is an account of decaying averages of past and past squared gradients:

$$m_t = \beta_1 m_{t-1} + (1-\beta_1) g_t, \tag{2}$$
$$v_t = \beta_2 v_{t-1} + (1-\beta_2) g_t^2, \tag{3}$$

with $m_t = \mathbb{E}[g_t]$ and $v_t = \mathbb{E}[g_t^2]$ being the mean and mean squared variance of the gradient g_t, and the decay rates β_1 and β_2.

We perform noise-free numerical simulations, on condition that the optimization algorithm has direct access to an exact value of energy, as though it was obtained with an infinite number of VQE shots. We found that for our problems, the optimal learning rate $\eta = 0.2$, the decay parameters are taken at the default values $\beta_1 = 0.9, \beta_2 = 0.999$. The gradients are estimated by finite differences. Each component of the gradient is estimated as $\partial_\theta\mathcal{E}(\theta_k) \approx (\mathcal{E}(\theta_k + \delta) - \mathcal{E}(\theta_k))/\delta$, where the parameter is chosen as $\delta = 10^{-6}$.

Probe states. Clearly, the performance of VQE crucially depends on the choice of ansatz state. Most common approach uses the unitary version of the coupled cluster method, the unitary coupled cluster ansatz [51, 52]. For interacting spin problems, the (non)unitary coupled cluster ansatz can be composed out of spin flip operators [53]. There is no direct evidence that this approach might be simulated on a classical computer in large scale, even when the series is truncated on low order terms [54]. In principle, a quantum computer could efficiently prepare this state truncated up to some kth using the SuzukiTrotter decomposition [55]. However, for a system of n qubits it requires $O(n^k)$ unitary gates, making this technique out of reach for contemporary quantum computers. Here we use a heuristic ansatz which consists of layers of parametrized two-qubit gates acting alternatively either on pairs $(1,2), (3,4), ..., (2k-1, 2k)$ or on pairs $(2,3), (4,5), ..., (2k, 2k+1)$. We will refer to this construction as a checkerboard ansatz.

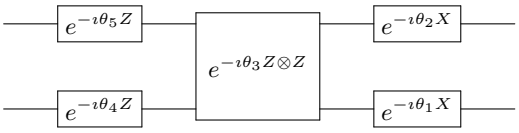

FIG. 1. A two-qubit entangler gate is sandwiched by universal one-qubit rotation, parametrized by θ_1, θ_2, θ_4, and θ_5, and a two-qubit gate, parametrized by θ_3.

In this work, we will use two different families of two-qubit gates. One is a generic combination of single- and two-qubit rotations depicted in Fig. 1. Written out explicitly, this gate reads:

$$U(\boldsymbol{\theta}) = (\mathcal{R}_z(\theta_5) \otimes \mathcal{R}_z(\theta_4)) \circ \\ \circ \mathcal{R}_{zz}(\theta_3) \circ (\mathcal{R}_x(\theta_2) \otimes \mathcal{R}_x(\theta_1)), \tag{4}$$

where $\mathcal{R}_x(\xi) = e^{-\imath\xi X}$, $\mathcal{R}_z(\xi) = e^{-\imath\xi Z}$, and $\mathcal{R}_{zz}(\xi) = e^{-\imath\xi Z\otimes Z}$. The other two-qubit gate is a more subtle construction [11]:

$$U(\theta_1, \theta_2) = \begin{pmatrix} 1 & 0 & 0 & 0 \\ 0 & \cos\theta_1 & e^{\imath\theta_2}\sin\theta_1 & 0 \\ 0 & e^{-\imath\theta_2}\sin\theta_1 & -\cos\theta_1 & 0 \\ 0 & 0 & 0 & 1 \end{pmatrix}. \tag{5}$$

When a fermion problem is cast into a spin problem using the Jordan–Wigner mapping, this construction conserves the total number of particles by keeping the $|00\rangle$ and $|11\rangle$ subspaces invariant. Of course, to start with the desired number of particles, one has to initialize the qubits by applying the Pauli X gate. In principle, by adjusting the chemical potential, one already sets the number of particles seen in the ground state, but the ansatz restriction also excludes the exploration of the undesired states.

Spin-fermion mapping. In fermionic Hamiltonians, one has to keep track of the canonical anti-commutation relations. In contrast, qubits in a quantum computer are dis-

tinguishable particles that have no such relations. Therefore, in order to solve eigenvalue problems for a fermionic system on a quantum computer, one has to map one to another. One method to do that is known as the Jordan–Wigner transformation. Population-wise, the j-th electron site is mapped to j-th qubit. The mapping of the fermionic operators to qubit operators, though, carries the parity information in the form of a phase multiplier. Thus, fermionic creation and annihilation operators $f_j^\dagger$, f_j transform by the following rule:

$$f_j^\dagger = \mathcal{Z}_j \otimes \sigma_j^+, \quad f_j = \mathcal{Z}_j \otimes \sigma_j^-, \tag{6}$$

provided that $\mathcal{Z}_j = Z_1 \otimes .. \otimes Z_{j-1}$ and $\sigma^\pm = (X \pm iY)/2$. The order of site enumeration is important. For one-dimensional systems the procedure is clear enough, whereas for higher-dimensional systems one can enumerate the sites in a *snake* order, see e.g. [30] and references therein. The advantage of this technique is found in the ease with which one can enforce the total particle number. Nevertheless, the locality of the operators changes dramatically in order to contain the parity information. Typically, local fermionic operators map to n-local spin operators.

Another version of spin-fermion mapping is provided by the Bravyi–Kitaev transformation [56]. In this method, the population and parity information are mixed in a procedure that allows the fermionic operators to map to $\log n$ – local spin operators. However, under this transformation, there is no obvious way to enforce particle number conservation, except for adding extra penalty terms to the Hamiltonian.

Interacting spinless fermions. We apply the methodology described in previous sections to study the ground state properties of interacting quantum many-body systems. Consider the Hamiltonian of one-dimensional spinless fermions

$$H = -t \sum_{\langle i,j \rangle} c_i^\dagger c_j + V_1 \sum_i n_i n_{i+1} + V_2 \sum_i n_i n_{i+2}, \tag{7}$$

where $c_i^\dagger$, c_i stand for creation, annihilation operators of an electron at ith site with a number of $n(i) = c_i^\dagger c_i$ electrons, t is the hopping energy, V_1 and V_2 are nearest- and next-nearest-neighbor Coulomb interactions. In the first term, the summation $\langle \ldots \rangle$ is implied over nearest neighboring sites. In the following, we impose periodic boundary conditions. Earlier numerical studies suggest that when the V_2 is increased, on condition the ratio $V_1/V_2 = 2$ is fixed, this model is characterized by appearance of a metallic state but does not belong to the Luttinger liquid class [40]. Away from this ratio, the model is gapped. For $V_2 = 0$, a regular interacting model of spinless fermions is recovered.

We numerically test the difference between exact solution and the VQE solution for $V_2 = t, V_1 = 2t$ for different numbers of qubits and ansatz layers. In particular, Fig. 2 illustrates how efficiently the model with next-nearest-neighbor interactions is minimized by VQE. Clearly, more layers are needed to achieve the same accuracy for more qubits, although the exact scaling remains unclear. Notably, for 10 qubits, the energy error remains roughly the same despite the increase in the number of layers.

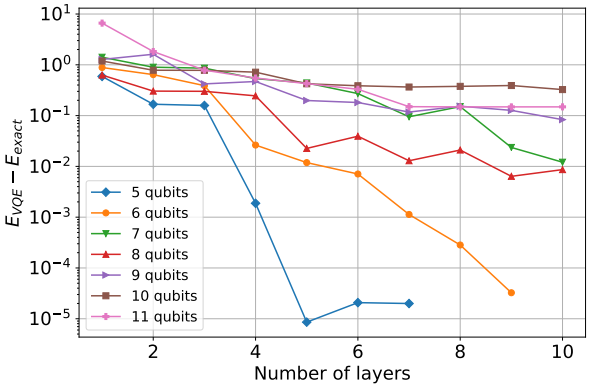

FIG. 2. Convergence of the VQE solution to the true ground state for the model of Eq. (7) versus the number of layers, on condition $V_1 = 2t, V_2 = t$. Cases of $n \leq 4$ qubits are not shown as they converged to exact solution within 2 layers.

We then estimated the velocities of density (v_S), current (v_J) and charge (v_N) excitations, using the finite-difference formulas given in Ref. [40] (Table I). For a Luttinger liquid, the fraction $v_S/v_N = v_J/v_S$, whereas the results of exact diagonalization results in this equality does not hold in the thermodynamic limit. The VQE numbers show certain similarity with the exact ones, however, for density excitations, the result is nowhere near the exact energy. This is likely caused by the extra term in the Hamiltonian introduced to constrain the momentum of the solution in analogy to Ref. [11] (see Supplemental Material for more details).

Correlation function. The energy error can be shown to be closely related to the infidelity between the true ground state and the variational approximation [57]. In other words, the error in energy is close to zero if the variational solution lies close to the ground state subspace. However, both of these metrics are useful only when we possess enough information on the exact solution. Since in real applications we want to find the true energy in the first place, we cannot assume this knowledge *a priori*. It is therefore also interesting to consider the convergence of other physically relevant observables. Specifically, we consider the convergence of the density-density correlation function $C(m) = \langle \hat{n}(0)\hat{n}(m) \rangle - \langle \hat{n}(0) \rangle \langle \hat{n}(m) \rangle$. Results of numerical simulations are shown in Fig. 3. We depict how this function depends on the qubit number i and the number of layers. The curves show qualitatively

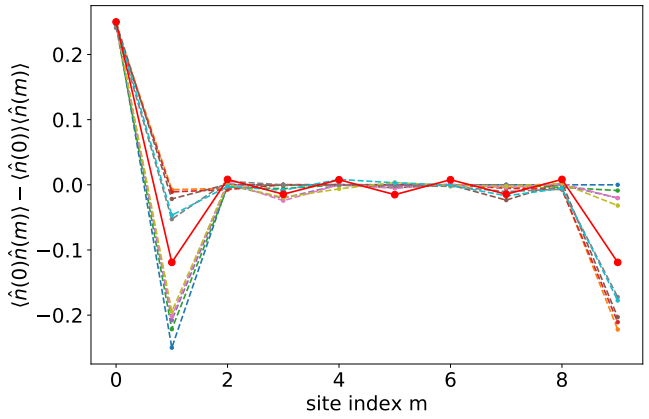

FIG. 3. Density-density correlation function between spatially separated lattice sites. Filled dots denote exact values as obtained by virtue of exact diagonalization of the Hamiltonian (7), dashed lines denote different approximations. Here $V_1 = 2t, V_2 = t$.

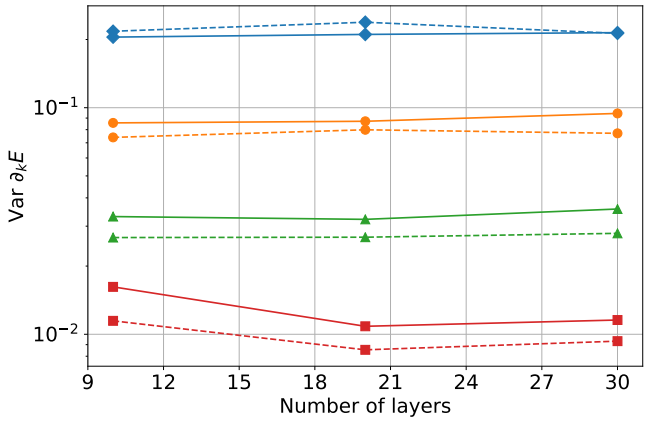

FIG. 4. Barren plateau effect for the Hamiltonian of Eq. (7) with $V_1 = t$ and $V_2 = 0$ (dashed lines), as well as $V_1 = 2t$ and $V_2 = t$ (solid lines) versus the number of qubits as realized by virtue of Jordan–Wigner mapping. Diamonds: 4 qubits; circles: 6 qubits; triangles: 8 qubits; squares: 10 qubits. Markers in Figs. 5 and 6 follow the same convention.

similar behavior even for small number of layers. However, a substantial decrease in error is observed only at 8 layers of the ansatz. Remarkably, for the VQE solution with the largest circuit depth one can fit the density-density correlation function with

$$C(m) \propto (-1)^m m^{-2.2}, \tag{8}$$

which algebraically decays with the lattice site index m. For the exact solution, the power of the decay is found to be 2.4 while the percentage error scales as $\mathcal{O}(m^{1/5})$.

Barren plateaus in VQE optimization. It was noticed in Ref. [44] that, given a long enough parametrized ansatz, the gradients of any reasonable cost function will be exponentially small with respect to the number of

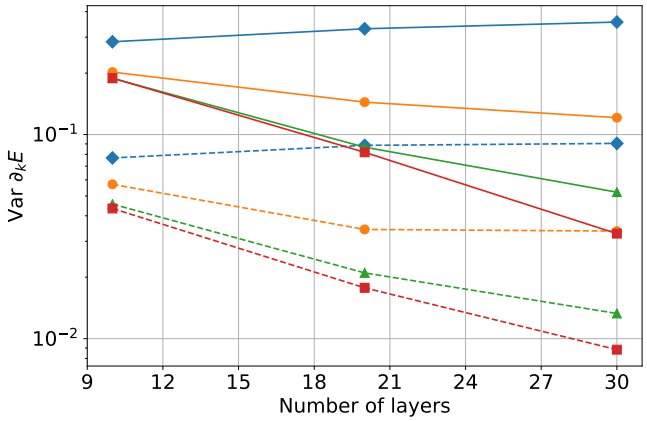

FIG. 5. Barren plateau effect for the Hamiltonian of Eq. (7) with $V_1 = t$ and $V_2 = 0$ (dashed lines), as well as $V_1 = 2t$ and $V_2 = t$ (solid lines) depending on the number of qubits as performed by means of Bravyi–Kitaev transformation.

qubits. Further on, it was discussed that for intermediate size quantum circuits, the onset of this *barren plateau* effect depends on the nature of the cost function [45]. In particular, two types of gradient behavior have been highlighted:

1. Var $\partial_\theta \mathcal{E}(\boldsymbol{\theta}) \in \mathcal{O}(e^{-L})$, where L is the number of ansatz layers. In this case, one can use a logarithmic number of layers without hitting the plateau.

2. Var $\partial_\theta \mathcal{E}(\boldsymbol{\theta}) \in \mathcal{O}(2^{-n})$ independent of the number of layers. In this case, the plateau is reached, thwarting VQE performance unless the initial conditions are somehow favorable.

In the following, we examine how this effect takes places in the VQE process for the model of Eq. (7). To do that, we estimate the values of the gradient components in $N = 50$ random points in the parameter space for some values of depths and qubit numbers.

In the case of one-dimensional interacting spinless fermions with the Hamiltonian (7), the variance both inside and outside the Luttinger liquid regime, mapped onto qubit space by Jordan-Wigner and Bravyi-Kitaev transformations, are respectively shown in Figs. 4 and 5. Surprisingly enough, we do not observe substantial difference in behavior of gradient variance when the model parameters are changed. The fermion-to-qubit mapping, however, impacted the results significantly. For Jordan–Wigner mapping, the exponential dependence on the qubit number emerges right away regardless of the layer number. For Bravyi–Kitaev mapping, the barren plateau regime set on more gradually.

To emphasize the difference, we consider how the barren plateaus arise in the Ising model with transverse mag-

Method	$E_0(n,N)$	$E_0(n,N+1)$	$E_0(n,N-1)$	$E_a(n,N)$	$E_{1P}(n,N)$	v_S	v_J	v_N
Exact	−2.626	0.654	−4.138	−2.346	−1.099	2.672	1.960	6.191
VQE (largest depth)	−2.477	0.729	−4.026	−2.270	4.320	10.819	1.318	4.922

TABLE I. Properties of the model specified by the Hamiltonian (7) evaluated by exact diagonalization and by VQE. These formulas require simple ground state energies $E_0(n,N)$ of a chain with n sites and N particles, ground state energy $E_a(n,N)$ for anti-periodic boundary conditions, and the energy of a state with lowest nonzero momentum $E_{1P}(n,N)$, as listed in Ref. [40]. The discrepancy in $E_{1P}(nN)$ between the results of exact diagonalization and VQE is associated with the fact that the latter accounts for the term that ensures the given momenta explicitly. Being devised to deal with local Hamiltonian mostly this dramatically affects convergence properties of VQE.

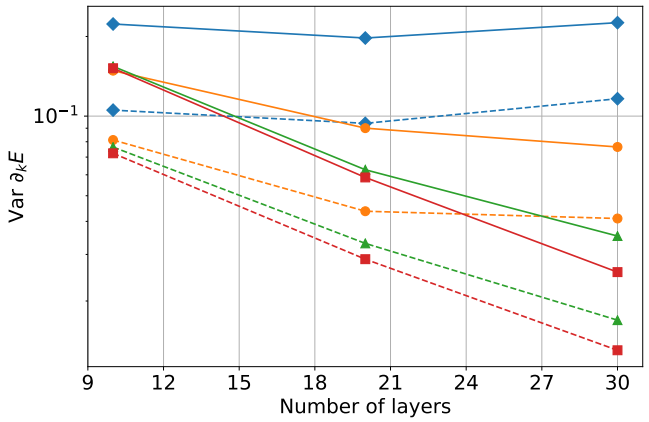

FIG. 6. Barren plateau effect for the transverse field Ising model of Eq. (9) away from criticality with $h = 0.1$ (dashed lines) and at the critical point $h = 1$ (solid lines).

netic field h:

$$H_{\mathrm{TFIM}} = \sum_i Z_i Z_{i+1} + h \sum_i X_i. \tag{9}$$

For this model we use a simpler two-qubit entangler gate shown in Fig. 1, owing to the fact that no fermion mappings are used and particle conservation is irrelevant. The gradient behavior away from the critical point ($h = 0.1$) and at the critical point ($h = 1$) is shown in Fig. 6. In this case, the gradient variance decays exponentially with the number of layers until reaching the plateau regime for the particular number of qubits. Thus, for 4 qubits the plateau is reached right away, while for 10 qubits 30 layers of the ansatz are still a number belonging to the transition regime. In the meantime, the criticality of the model does not seem to affect this behavior.

Discussion and conclusion. In this work, we studied the performance of the VQE when applied to one-dimensional spinless fermions with competing nearest- and next-nearest-neighbor interactions. Apart from considering the convergence with respect to energy, we have also considered density-density correlation function. This revealed that qualitative information can be recovered even if the VQE solution is relatively far from the true ground state energy. The correlation function decay was fit with a power law with an exponent close to the one found by exact diagonalization, although for large m the tails of these power law functions would be quite different.

We also performed numerical tests related to the onset of the barren plateau effect [44]. We discovered that fermion-to-qubit mapping is a key factor in the appearance of this effect. This result is consistent with the findings of Ref. [45], which connects the susceptibility to plateau with the locality of the Hamiltonian. Indeed, due to trailing Z's, Jordan–Wigner transformation produces terms which are acting on up to n qubits, while Bravyi–Kitaev transformation returns operators which act on $\mathcal{O}(n \log n)$ qubits each. This implies that using the Bravyi–Kitaev transformation may offer better convergence for problems with larger qubit numbers.

In general, given a VQE solution, one can query the expected values of any observables that can be constructed with a polynomial number of Pauli strings. For example, it was proposed to make use of $\Delta = \langle H^2 \rangle - \langle H \rangle^2$ in order to see the proximity to some eigenstate [34]. However, any two- and many-body correlation functions can be constructed this way, opening up an avenue to measure multipartite entanglement which is, however, characterized by non-polynomial computational complexity [58]. If nonetheless quantum entanglement is known, one might hope to be able to reconstruct the collective degrees of freedom by a careful study of entanglement of a wave function in the basis of individual spins/electrons.

Acknowledgments. We gratefully acknowledge fruitful discussions with M. I. Katsnelson. The work of AU and DY was supported by Russian Foundation for Basic Research Project No. 19-31-90159. Numerical simulations were performed using Qiskit. The Jordan–Wigner and Bravyi–Kitaev transformations were done with the use of OpenFermion.

* http://quantum.skoltech.ru; alexey.uvarov@skoltech.ru

[1] G. Carleo, I. Cirac, K. Cranmer, L. Daudet, M. Schuld, N. Tishby, L. Vogt-Maranto, and L. Zdeborová, Rev. Mod. Phys. **91**, 045002 (2019).

[2] T. Westerhout, N. Astrakhantsev, K. S. Tikhonov, M. I. Katsnelson, and A. A. Bagrov, Nat. Commun. **11**, 1593 (2020).

[3] J. Biamonte, P. Wittek, N. Pancotti, P. Rebentrost, N. Wiebe, and S. Lloyd, Nature **549**, 195 (2017).

[4] J. R. McClean, J. Romero, R. Babbush, and A. Aspuru-Guzik, New J. Phys. **18**, 023023 (2016).

[5] J. Li, X. Yang, X. Peng, and C.-P. Sun, Phys. Rev. Lett. **118**, 150503 (2017).

[6] Y. Li and S. C. Benjamin, Phys. Rev. X **7**, 021050 (2017).

[7] K. Temme, S. Bravyi, and J. M. Gambetta, Phys. Rev. Lett. **119**, 180509 (2017).

[8] J. I. Colless, V. V. Ramasesh, D. Dahlen, M. S. Blok, M. E. Kimchi-Schwartz, J. R. McClean, J. Carter, W. A. de Jong, and I. Siddiqi, Phys. Rev. X **8**, 011021 (2018).

[9] R. Babbush, N. Wiebe, J. McClean, J. McClain, H. Neven, and G. K.-L. Chan, Phys. Rev. X **8**, 011044 (2018).

[10] I. D. Kivlichan, J. McClean, N. Wiebe, C. Gidney, A. Aspuru-Guzik, G. K.-L. Chan, and R. Babbush, Phys. Rev. Lett. **120**, 110501 (2018).

[11] P. K. Barkoutsos, J. F. Gonthier, I. Sokolov, N. Moll, G. Salis, A. Fuhrer, M. Ganzhorn, D. J. Egger, M. Troyer, A. Mezzacapo, S. Filipp, and I. Tavernelli, Phys. Rev. A **98**, 022322 (2018).

[12] A. Macridin, P. Spentzouris, J. Amundson, and R. Harnik, Phys. Rev. Lett. **121**, 110504 (2018).

[13] N. Klco, E. F. Dumitrescu, A. J. McCaskey, T. D. Morris, R. C. Pooser, M. Sanz, E. Solano, P. Lougovski, and M. J. Savage, Phys. Rev. A **98**, 032331 (2018).

[14] K. Setia and J. D. Whitfield, J. Chem. Phys. **148**, 164104 (2018).

[15] T. Jones, S. Endo, S. McArdle, X. Yuan, and S. C. Benjamin, Phys. Rev. A **99**, 062304 (2019).

[16] H. R. Grimsley, S. E. Economou, E. Barnes, and N. J. Mayhall, Nat. Commun. **10**, 3007 (2019).

[17] M. Ganzhorn, D. J. Egger, P. Barkoutsos, P. Ollitrault, G. Salis, N. Moll, M. Roth, A. Fuhrer, P. Mueller, S. Woerner, I. Tavernelli, and S. Filipp, Phys. Rev. Applied **11**, 044092 (2019).

[18] R. M. Parrish, E. G. Hohenstein, P. L. McMahon, and T. J. Martínez, Phys. Rev. Lett. **122**, 230401 (2019).

[19] P. L. Dallaire-Demers, J. Romero, L. Veis, S. Sim, and A. Aspuru-Guzik, Quantum Sci. Technol. **4**, 045005 (2019).

[20] T. Takeshita, N. C. Rubin, Z. Jiang, E. Lee, R. Babbush, and J. R. McClean, Phys. Rev. X **10**, 011004 (2020).

[21] M. Lubasch, J. Joo, P. Moinier, M. Kiffner, and D. Jaksch, Phys. Rev. A **101**, 010301 (2020).

[22] V. Akshay, H. Philathong, M. E. S. Morales, and J. D. Biamonte, Physical Review Letters **124**, 090504 (2020).

[23] A. Peruzzo, J. McClean, P. Shadbolt, M.-H. Yung, X.-Q. Zhou, P. J. Love, A. Aspuru-Guzik, and J. L. O'Brien, Nat. Commun. **5**, 4213 (2014).

[24] P. J. J. O'Malley, R. Babbush, I. D. Kivlichan, J. Romero, J. R. McClean, R. Barends, J. Kelly, P. Roushan, A. Tranter, N. Ding, B. Campbell, Y. Chen, Z. Chen, B. Chiaro, A. Dunsworth, A. G. Fowler, E. Jeffrey, A. Megrant, J. Y. Mutus, C. Neill, C. Quintana, D. Sank, A. Vainsencher, J. Wenner, T. C. White, P. V. Coveney, P. J. Love, H. Neven, A. Aspuru-Guzik, and J. M. Martinis, Phys. Rev. X **6**, 10.1103/PhysRevX.6.031007 (2016).

[25] Y. Li, J. Hu, X.-M. Zhang, Z. Song, and M.-H. Yung, Adv. Theory Simul. **2**, 1800182 (2019).

[26] Y. Cao, J. Romero, J. P. Olson, M. Degroote, P. D. Johnson, M. Kieferová, I. D. Kivlichan, T. Menke, B. Peropadre, N. P. D. Sawaya, S. Sim, L. Veis, and A. Aspuru-Guzik, Chem. Rev. **119**, 10856 (2019).

[27] A. Kandala, A. Mezzacapo, K. Temme, M. Takita, M. Brink, J. M. Chow, and J. M. Gambetta, Nature , 242 (2017).

[28] Y. Nam, J.-S. Chen, N. C. Pisenti, K. Wright, C. Delaney, D. Maslov, K. R. Brown, S. Allen, J. M. Amini, J. Apisdorf, K. M. Beck, A. Blinov, V. Chaplin, M. Chmielewski, C. Collins, S. Debnath, A. M. Ducore, K. M. Hudek, M. Keesan, S. M. Kreikemeier, J. Mizrahi, P. Solomon, M. Williams, J. D. Wong-Campos, C. Monroe, and J. Kim, arXiv:1902.10171 (2019).

[29] C. Hempel, C. Maier, J. Romero, J. McClean, T. Monz, H. Shen, P. Jurcevic, B. P. Lanyon, P. Love, R. Babbush, A. Aspuru-Guzik, R. Blatt, and C. F. Roos, Phys. Rev. X **8**, 10.1103/PhysRevX.8.031022 (2018).

[30] C. Cade, L. Mineh, A. Montanaro, and S. Stanisic, arXiv:1912.06007 (2019).

[31] E. Grant, L. Wossnig, M. Ostaszewski, and M. Benedetti, Quantum **3**, 214 (2019).

[32] S. Endo, I. Kurata, and Y. O. Nakagawa, arXiv:1909.12250 (2019).

[33] C. Bravo-Prieto, J. Lumbreras-Zarapico, L. Tagliacozzo, and J. I. Latorre, arXiv:2002.06210 (2020).

[34] C. Kokail, C. Maier, R. van Bijnen, T. Brydges, M. K. Joshi, P. Jurcevic, C. A. Muschik, P. Silvi, R. Blatt, C. F. Roos, and P. Zoller, Nature **569**, 355 (2019).

[35] E. Farhi, J. Goldstone, and S. Gutmann, arXiv:1411.4028 (2014).

[36] G. Nannicini, Phys. Rev. E **99**, 013304 (2019).

[37] I. Rungger, N. Fitzpatrick, H. Chen, C. H. Alderete, H. Apel, A. Cowtan, A. Patterson, D. M. Ramo, Y. Zhu, N. H. Nguyen, and et al., arXiv:1910.04735 [cond-mat, physics:quant-ph] (2019).

[38] B. Jaderberg, A. Agarwal, K. Leonhardt, M. Kiffner, and D. Jaksch, arXiv:2002.04612 [quant-ph] (2020), arXiv: 2002.04612.

[39] A. K. Zhuravlev, M. I. Katsnelson, and A. V. Trefilov, Phys. Rev. B **56**, 12939 (1997).

[40] A. K. Zhuravlev and M. I. Katsnelson, Phys. Rev. B **61**, 15534 (2000).

[41] A. K. Zhuravlev and M. I. Katsnelson, Phys. Rev. B **64**, 033102 (2001).

[42] M. Hohenadler, S. Wessel, M. Daghofer, and F. F. Assaad, Phys. Rev. B **85**, 195115 (2012).

[43] C. Karrasch and J. E. Moore, Phys. Rev. B **86**, 155156 (2012).

[44] J. R. McClean, S. Boixo, V. N. Smelyanskiy, R. Babbush, and H. Neven, Nat. Commun. **9**, 4812 (2018).

[45] M. Cerezo, A. Sone, T. Volkoff, L. Cincio, and P. J. Coles, arXiv:2001.00550 (2020).

[46] K. Mitarai, Y. O. Nakagawa, and W. Mizukami, Phys. Rev. Research **2**, 013129 (2020).

[47] M. Schuld, V. Bergholm, C. Gogolin, J. Izaac, and N. Killoran, Phys. Rev. A **99**, 032331 (2019).

[48] R. Sweke, F. Wilde, J. Meyer, M. Schuld, P. K. Fährmann, B. Meynard-Piganeau, and J. Eisert, arXiv:1910.01155 (2019).

[49] A. Harrow and J. Napp, arXiv:1901.05374 (2019).

[50] D. P. Kingma and J. Ba, arXiv:1412.6980 (2017).

[51] Y. Shen, X. Zhang, S. Zhang, J.-N. Zhang, M.-H. Yung, and K. Kim, Phys. Rev. A **95**, 020501 (2017).

[52] E. F. Dumitrescu, A. J. McCaskey, G. Hagen, G. R. Jansen, T. D. Morris, T. Papenbrock, R. C. Pooser, D. J.

Dean, and P. Lougovski, Phys. Rev. Lett. **120**, 210501 (2018).
[53] O. Götze, D. J. J. Farnell, R. F. Bishop, P. H. Y. Li, and J. Richter, Phys. Rev. B **84**, 224428 (2011).
[54] A. G. Taube and R. J. Bartlett, Int. J. Quantum Chem. **106**, 3393 (2006).
[55] M. Suzuki, Prog. Theor. Phys. **56**, 1454 (1976).
[56] S. Bravyi and A. Kitaev, Ann. Phys. **298**, 210 (2002).
[57] J. Biamonte, arXiv:1903.04500 (2019).
[58] G. De Chiara and A. Sanpera, Rep. Prog. Phys. **81**, 074002 (2018).

SUPPLEMENTAL MATERIAL: EVALUATION OF EXCITATION VELOCITIES USING VQE

To estimate how useful VQE is for condensed matter systems, particularly one-dimensional chain of spinless fermions with nearest- and next-nearest neighbors interactions, we provide numerical methodology for computing the velocities of density (v_S), current (v_J), and charge (v_N) excitations. These velocities are estimated using the finite-difference formulas given in [40] and require knowledge of ground state energies $E_0(n, N)$ of a chain with n sites and N particles, ground state energy $E_a(n, N)$ for anti-periodic boundary conditions, and the energy of a state with lowest nonzero momentum $E_{1P}(n, N)$.

i) The energy $E_0(n, N)$ is what VQE tries to find by definition, no extra actions are needed.

ii) The energy $E_a(n, N)$ requires an adjustment of the Hamiltonian to account for anti-periodic boundary conditions: $\psi(x + n) = -\psi(x)$. For the Hamiltonian, this means that the operator acting on the $(n + 1)$'th site differs from that acting on the first site just by the sign: $c_{n+1} = -c_1$. In the Hubbard model Hamiltonian, this amounts to changing the sign of the hopping term between the first and the last sites. The rest of the VQE procedure goes in a standard way.

iii) To compute the energy $E_{1P}(n, N)$, we need to pose restrictions on the momentum that the ansatz can generate. To do this, we recall that the momentum creation and annihilation operators are connected with site creation and annihilation operators via the Fourier transform:

$$a_k = \frac{1}{\sqrt{n}} \sum_{j=1}^{n} e^{ikj} a_j$$

Now, the population of the state with momentum k is determined by $a_k^\dagger a_k$, the total momentum operator can be written as $\hat{p} = \sum_k k a_k^\dagger a_k$ for $k \in \{2\pi/L \cdot (\lfloor -L/2 \rfloor + 1), ..., 2\pi/L \cdot \lfloor L/2 \rfloor\}$. With that operator, we minimize the Hamiltonian $H' = H + C(\hat{p} - p_{target})^2$. The value of C should be large enough to enforce this restriction. We took $C = 10$. To do that, we remember that the hopping Hamiltonian $H_{hop} = -t \sum c_i^\dagger c_{i+1} + h.c.$ is in fact the Hamiltonian corresponding to kinetic energy $\sum p_i^2/2$.